



LJMU Research Online

Petkar, KC, Chavhan, S, Kunda, N, Saleem, IY, Somavarapu, S, Taylor, KMG and Sawant, KK

Development of Novel Octanoyl Chitosan Nanoparticles for Improved Rifampicin Pulmonary Delivery: Optimization by Factorial Design

<http://researchonline.ljmu.ac.uk/id/eprint/9068/>

Article

Citation (please note it is advisable to refer to the publisher's version if you intend to cite from this work)

Petkar, KC, Chavhan, S, Kunda, N, Saleem, IY, Somavarapu, S, Taylor, KMG and Sawant, KK (2018) Development of Novel Octanoyl Chitosan Nanoparticles for Improved Rifampicin Pulmonary Delivery: Optimization by Factorial Design. AAPS PharmSciTech. 19 (4). pp. 1758-1772. ISSN 1530-

LJMU has developed [LJMU Research Online](http://researchonline.ljmu.ac.uk/) for users to access the research output of the University more effectively. Copyright © and Moral Rights for the papers on this site are retained by the individual authors and/or other copyright owners. Users may download and/or print one copy of any article(s) in LJMU Research Online to facilitate their private study or for non-commercial research. You may not engage in further distribution of the material or use it for any profit-making activities or any commercial gain.

The version presented here may differ from the published version or from the version of the record. Please see the repository URL above for details on accessing the published version and note that access may require a subscription.

For more information please contact researchonline@ljmu.ac.uk

<http://researchonline.ljmu.ac.uk/>

Development of Novel Octanoyl Chitosan Nanoparticles for Improved Rifampicin Pulmonary Delivery: Optimization by Factorial Design

Kailash C. Petkar,^{1,2} Sandip Chavhan,¹ N. Kunda,³ I. Saleem,³ S. Somavarapu,² Kevin M. G. Taylor,² and Krutika K. Sawant^{1,4}

Abstract. A novel hydrophobic chitosan derivative, octanoyl chitosan (OC) with improved organic solubility was synthesized, characterized, and employed for the preparation of rifampicin (Rif) encapsulated nanoparticle formulations for pulmonary delivery. OC was characterized to confirm acyl group substitution and cytotoxicity in A549 epithelial lung cells. OC nanoparticles were produced by the double emulsion solvent evaporation technique without cross-linking and characterized for particle size distribution, morphology, crystallinity, thermal stability, aerosol delivery, and drug release rate. OC was successfully synthesized with substitution degree of $44.05 \pm 1.75\%$, and solubility in a range of organic solvents. Preliminary cytotoxicity studies of OC showed no effect on cell viability over a period of 24 h on A549 cell lines. OC nanoparticles were optimized using a 3^2 full factorial design. An optimized batch of OC nanoparticles, smooth and spherical in morphology, had mean hydrodynamic diameter of 253 ± 19.06 nm (PDI 0.323 ± 0.059) and entrapment efficiency of $64.86 \pm 7.73\%$ for rifampicin. Pulmonary deposition studies in a two-stage impinger following aerosolization of nanoparticles from a jet nebulizer gave a fine particle fraction of $43.27 \pm 4.24\%$. *In vitro* release studies indicated sustained release ($73.14 \pm 3.17\%$) of rifampicin from OC nanoparticles over 72 h, with particles demonstrating physical stability over 2 months. In summary, the results confirmed the suitability of the developed systems for pulmonary delivery of drugs with excellent aerosolization properties and sustained-release characteristics.

KEY WORDS: octanoyl chitosan; hydrophobic chitosan; rifampicin; factorial design; tuberculosis.

INTRODUCTION

Being the second leading cause of death worldwide from infectious diseases, after the human immunodeficiency virus (HIV) (1), tuberculosis (TB) is continuously posing a major global health problem. The latest estimate by the World Health Organization (WHO) indicated 10.4 million new cases of TB in 2016, of which 6.8 and 1.5 million cases,

corresponding to 65 and 15%, were among men and women respectively, while 1.0 million (10%) were among children. People having co-infection of HIV with TB were calculated to be 1.2 million (10%) of all new TB cases, while drug-resistant TB is a continued threat (1). Currently, chemotherapy is the only available option for the treatment of TB. However, it has several limitations such as lengthy treatment (requiring combination antibiotics therapy daily for 6–9 months), patient non-compliance, non-localized delivery, worsening of the disease due to co-infection with HIV and generation of drug-resistant mutants of TB bacilli. Moreover, high dose, dosing frequency, and adverse side effects are other major factors limiting the effectiveness of the current TB chemotherapy (2). Among several anti-TB drugs, rifampicin (RIF) is one of the most effective and is an important component of DOTS (directly observed treatment, short-course) therapy. It is considered a model anti-TB drug, with well-defined chemical and physical properties. However, a series of limitations such as low bioavailability, enhanced drug resistance, less cell permeability, inability to achieve adequate drug concentrations at the infected site, and degradation before reaching the target site have impeded its effectiveness

Electronic supplementary material The online version of this article (<https://doi.org/10.1208/s12249-018-0972-9>) contains supplementary material, which is available to authorized users.

¹ Faculty of Pharmacy, Department Pharmaceutics, The Maharaja Sayajirao University of Baroda, Vadodara, 390001, Gujarat, India.

² Department of Pharmaceutics, UCL School of Pharmacy, Brunswick Square, London, WC1N 1AX, UK.

³ School of Pharmacy, Liverpool John Moores University, Liverpool, UK.

⁴ To whom correspondence should be addressed. (e-mail: dr_krutikasawant@rediffmail.com)

(2). Therefore, developing an alternative delivery system and route of administration for rifampicin would clearly be advantageous.

The inhaled route of administration is receiving increasing attention for direct and target specific delivery of drug to the lungs due to the large alveolar surface area, extensive vascularization, limited proteolytic activity, avoidance of first-pass metabolism, and rapid onset of drug action (3). However, lack of retention of drugs in the lungs and some invasive procedures for drug administration have hindered its clinical application (2). Sustained and targeted drug delivery to the pulmonary site is usually achieved by formulating drugs in micro- or nanoparticle structures, which can be administered as a therapeutic aerosol. Formulation of anti-TB drug into nanoparticulate carrier system for pulmonary delivery could help to solve these issues associated with their current use. The small-sized colloidal nanoparticles have easy penetration into the alveoli, may have enhanced alveolar macrophage uptake compared to microparticles and can achieve an effective therapeutic outcome (4,5).

Several polymers have been employed for the preparation of nanoparticles for pulmonary delivery including, polylactic-co-glycolic acid, polycaprolactone, chitosan, and alginates. (6,7) Chitosan, a natural polymer, consisting mainly of β (1 \rightarrow 4)-linked D-glucosamine and *N*-acetyl β -D-glucosamine, has been widely used owing to its advantages such as biodegradability, biocompatibility, mucoadhesive property (due to positive charge in aqueous environments), low toxicity, and antimicrobial activity (8). Moreover, improved entrapment and uptake by the alveolar macrophages for effective targeting has made this polymer a choice for the lung delivery (4). There are reports demonstrating application of chitosan microparticles and nanoparticles for delivery of drugs and macromolecules to the lung (9–12). However, loss of their positive surface charge, aggregate formation at physiologic pH, and their inability to protect and control the release of small molecular drugs have contributed to chitosan's current limited applications in drug delivery (13,14). Various chemical modifications of chitosan have been investigated in order to overcome these limitations by conjugating hydrophobic and hydrophilic groups (owing to the presence of reactive amine and hydroxyl groups) for application in drug/protein delivery (12,15). Modification of chitosan by acylation (using acyl chlorides and anhydrides) confers organic solubility and an ester linkage is hydrolyzable by enzymes such as lipase (13). Several methods for synthesizing hydrophobic chitosan derivatives for biomedical applications have been reported (12,16–18), while nanoparticles were produced mainly by cross-linking, drying, reverse micellar, or emulsion cross-linking. The cross-linking method often involves the use of potential toxic agents such as glutaraldehyde, making this methodology less effective and tedious due to post-formulation removal of cross-linking agents. To the best of our knowledge, there have been no reports exploring hydrophobic chitosan derivative (OC) for the preparation of nanoparticles by emulsification without cross-linking.

Thus, the present study describes the utilization of hydrophobic chitosan in the preparation of nanoparticles for pulmonary delivery of rifampicin using an emulsion solvent evaporation technique without cross-linking. The aim of the study was to produce suitably sized rifampicin-loaded octanoyl chitosan nanoparticles using a freeze-drying process, while

optimization of the formula was achieved by factorial design. MTT (3-(4,5-dimethylthiazol-2-yl)2,5-diphenyl tetrazolium bromide) assay indicated the suitability of the presented polymer for safe use in drug delivery. The physicochemical properties, loading capacity (LC), encapsulation efficiency (EE), and release properties of encapsulated rifampicin were investigated, while stability studies indicated the stability of the octanoyl chitosan nanoparticles. In sum, this study clearly demonstrated positively charged nanoparticles with a release-controlling ability of octanoyl chitosan, suggesting its suitability as a novel drug carrier for pulmonary delivery.

MATERIALS AND METHODS

Materials

Rifampicin was purchased from Sigma-Aldrich (St. Louis, USA). Chitosan oligosaccharide [MW > 5 kDa; degree of deacetylation (DDA) 80–90%] was supplied by Kitto Life Co. Ltd. (Kyongki-Do, Seoul, South Korea). Octanoyl chloride, methane sulfonic acid, sodium bicarbonate, Poloxamer F-127, and polyvinyl alcohol (PVA) were purchased from Sigma-Aldrich (St. Louis, USA). Cellulose dialysis tubing (Molecular weight cut-off 12–14,000 Da and 5000 Da) was purchased from Medicell International Ltd., (London, UK). Dimethyl sulfoxide (DMSO, anhydrous), methanol, ethanol, chloroform, dichloromethane (DCM), acetone and all other HPLC grade solvents were obtained from Sigma-Aldrich (St. Louis, USA).

Methods

Preparation of OC and OC-Rif Nanoparticles

Octanoyl chitosan was synthesized as per the method described by Huang et al. with modifications and confirmed using NMR and FTIR studies (14). The final product was further utilized to prepare nanoparticles (see supporting information).

OC nanoparticles were prepared using the double emulsion solvent evaporation technique as previously described (19). Accurately weighed (50 mg) OC was dissolved in 1.5 ml of dichloromethane. The required quantity of rifampicin (5–15 mg) was dissolved in this solution with agitation until complete dissolution. Organic phase was emulsified immediately with aqueous phase by sonication for 15 s at 15 Amp to form a primary emulsion. The emulsion obtained was then poured into 10 ml of aqueous phase containing 0.5% PVA (polyvinyl alcohol) and sonicated at 15 Amp for 30 s (Labsonic® P, Sartorius Biotech GmbH, Germany). The resultant multiple emulsion was magnetically stirred (RO 10 power IKA WERKE, Staufen, Germany) at 25–30 °C for about 4 h to completely evaporate the organic phase. Recovery of nanoparticles formed was achieved by centrifugation at 21000 rpm for 30 min (Sigma Laboratory Centrifuge, 3K30, UK). Samples were washed three times with fresh deionized water to remove any residual surfactant (PVA) and free drug. Nanoparticles obtained were then lyophilized (VirTis Co. Inc., UK) following addition of cryoprotectant, trehalose dehydrate (1% w/v) as described

by Holzer et al., (20). A similar protocol was followed to prepare blank OC NPs without rifampicin.

Optimization of Particle Size and Entrapment Efficiency by Factorial Design

Preliminary optimization was carried out to study the influence of process parameters such as sonication time, organic solvent, surfactant, and concentration of surfactant. Thereafter, blank OC NPs and rifampicin-loaded OC NPs (OC-Rif NPs) were prepared using a 3² randomized full factorial design. Accordingly, 9 possible combinations of experimental trials were prepared with three replicates. The concentration of polymer (X₁) and concentration of Rif (X₂) were selected as independent variables, while parameters mean particle size, MPS (Y₁), and entrapment efficiency, EE (Y₂), were selected as dependent variables (response parameters). The responses were analyzed by statistical modeling of interactive and polynomial terms. The response surface curves and contour plots were prepared to study the effects of independent variables. All the statistical operations were carried out using Design-Expert software, version 8.0.7.1 (Stat-Ease Inc., Minneapolis, USA), Statistica (StatSoft, Tulsa, USA) and Microsoft Excel 2010 (I) (Gurgaon, India). Independent factors at their varied combinations in terms of coded and their actual values are represented in Table I.

Optimization and Data Analysis. The optimization of parameters was carried out by applying response surface methodology (RSM) computations using Design Expert® software (version 8.0.5.2, Stat-Ease Inc., Minneapolis, MN), Statistica (Stat soft, Tulsa, USA), and Microsoft Excel 2010. Multiple regression analysis (MLRA) was used to generate polynomial models (including interaction and quadratic terms) for the response variable and its Eq. (1) can be presented as below.

$$Y = b_0 + b_1X_1 + b_2X_2 + b_3X_1^2 + b_4X_2^2 + b_5X_1X_2 + b_6X_1^2X_2 + b_7X_1X_2^2 \quad (1)$$

where b₀ is the intercept corresponding to the arithmetic average of quantitative outcomes of 9 runs, b₁ to b₇ signifies coefficients calculated from the experimentally observed values of Y, and X₁ and X₂ stands for the coded levels of the independent variables. The terms X₁X₂ represent interaction term, while X_i² (i = 1 to 2) denotes quadratic terms. The main effects, X₁ and X₂, symbolizes the mean outcome because of changing one factor at a time from its low to high value, while the interaction terms (X₁X₂) indicate changes in the response parameters when two factors are simultaneously changed. Non-linearity in the model was also investigated by the polynomial terms (X² and X²). The

polynomial equation as mentioned above was utilized to interpret the results based on the values of magnitude of coefficients and the accompanying positive (synergistic effect) or negative sign (antagonistic effect) (21).

Statistical validity of the polynomials was determined using ANOVA as provided in the Design-Expert® software (Stat-Ease,

USA) and Microsoft Excel 2010 (I) at a significance level of p < 0.05. In addition, 3D response surface curves, and the 2D contour plots were also developed by the Statistica® software (Stat Soft, Tulsa, USA). The best fitting mathematical model was chosen by comparing various statistical parameters such as the coefficient of variation (CV), the multiple correlation coefficient (R²), adjusted multiple correlation coefficient (Adj R²), and the predicted residual sum of squares (PRESS). For the chosen model, smaller the PRESS value in relation to the other models under consideration signifies how well the model fits the data (19).

Characterization of OC-Rif Nanoparticles

Mean Particle Size and Zeta Potential. Dynamic light scattering (DLS) and laser Doppler velocimetry (LDV) was employed to measure particle size (expressed as mean hydrodynamic diameter and polydispersity index; PDI) and surface charge (zeta potential) of the particles respectively using Zetasizer, Nanoseries Instrument (Nano 25, Malvern Instruments, Worcestershire, UK). The nanoparticles were re-dispersed in deionized water and bath sonicated (Ultrawave Ltd., UK) for 5 min and the resultant samples were examined for particle size and zeta potential.

Rifampicin Loading and Encapsulation Efficiency. Encapsulation of rifampicin in NPs was evaluated by dissolving OC-Rif NPs in methanol and analyzed using UV-VIS spectrophotometer. A known weight of Rif loaded nanoparticles was suspended in methanol, allowed to stand for around 10–15 min and water was added in a sufficient amount to precipitate OC. The suspension obtained was centrifuged (Bio Rad Centrifuge, UK) and the concentration of rifampicin in the supernatant was determined using UV-VIS spectrophotometer (Jenway UV/Vis Spectrophotometer, Staffordshire, UK) at 475 nm (22) (Benetton et al., 1998). Analysis was performed in triplicate for each batch of drug loaded NPs. The yield, drug loading and encapsulation efficiency were calculated using following formulae and presented as mean of each of the parameter:

$$\text{Yield } (\%) = \frac{\text{Weight of NP recovered}}{\text{Weight of Drug; polymer and excipient}} \times 100 \quad (2)$$

$$\text{Drug Loading } (\%) = \frac{\text{Weight of Rif in NP}}{\text{Weight of NP recovered}} \times 100 \quad (3)$$

$$\text{Entrapment Efficiency } (\%) = \frac{\text{Weight of Rif in NP}}{\text{Weight of Rif fed initially}} \times 100 \quad (4)$$

Morphology Determination by Scanning Electron Microscopy. Lyophilized nanoparticles were observed using scanning electron microscopy (SEM) to study their shape and surface morphology. The samples were mounted onto the

Table I. Factorial Design Parameters for Optimization of OC-Rif Nanoparticles

Independent Factors		Levels used, actual (coded value)								
		Low (- 1)			Medium (0)			High (+ 1)		
X ₁ —OC concentration (mg)		50			75			100		
X ₂ —Concentration of Rif (mg)		5			10			15		
Dependent variables		Constraint								
Y1 = Particle Size nm		Minimize								
Y2 = % EE		Maximize								
Formulation of the nanoparticles utilizing 3 ² factorial design (Coded values)										
Variables/batch no.	C1	C2	C3	C4	C5	C6	C7	C8	C9	
X ₁	- 1	- 1	- 1	0	0	0	+1	+1	+1	
X ₂	- 1	0	+ 1	- 1	0	+ 1	- 1	0	+ 1	

OC octanoyl chitosan

SEM sample holder and gold coated in a vacuum chamber and images were recorded at the required magnification at the acceleration voltage of 10 kV using FEI XL30 TMP Scanning electron microscope (FEI XL30 TMP, Philips, Netherlands).

Transmission Electron Microscopy. Nanoparticles were also visualized by transmission electron microscopy (TEM). Briefly, a drop of nanoparticle suspension was stained with phosphotungstic acid and placed on a coated carbon grid and vacuum dried. The grid was then examined immediately under TEM (Philips Electron Optics BV, Netherlands) and the electron micrographs were obtained.

Differential Scanning Calorimetry and X-ray Powder Diffraction Studies. A differential scanning calorimeter (DSC Q 2000, TA Instruments, USA) was used to determine the thermal properties of the freeze-dried nanoparticles (OC-Rif-NPs) and rifampicin. Correctly weighed samples (around 3–5 mg) of the stated materials were placed in hermetically sealed aluminum pans; a sealed empty aluminum pan was used as a reference. Heating runs for each sample were set from 10°C to 300°C at 10°C min⁻¹ in a nitrogen atmosphere to get the heating scan (thermographs). X-ray powder diffractometry was carried out using an X-ray diffractometer (Oxford Diffraction Xcalibur novaT, UK) and diffractograms obtained were analyzed to understand physical state of the powder. The samples were mounted on a sample holder and X-ray powder diffraction (XRD) patterns were recorded in the range of 5–50° at the speed of 5° per min.

Aerosolization and Aerosol Characterization Using Twin-Stage Impinger

The aerosolization of OC-Rif nanoparticle formulations was determined following nebulization using a TSI (Glass Impinger, Apparatus A Ph. Eur; Copley Scientific Ltd., Nottingham, UK) as per the specifications given in the European Pharmacopoeia (23). In brief, lyophilized OC-Rif NP samples (10 mg) were prepared by dispersing in 5 ml deionized water. The required volume (5 ml) was loaded into

a PariBoy air-jet nebulizer with Inhaler Boy compressor (Pari Medical, UK). The aerosol generated was directed into the TSI *via* a mouthpiece adaptor, and a vacuum pump set at a flow rate of 60 L/min was used to draw the aerosol through the impinger. The upper and lower stages (stage 1 and stage 2) of the TSI were filled with 7 and 30 ml of deionized water respectively. The nebulization was performed until aerosol generation stopped (nebulizer dryness). Thereafter, the nebulizer was gently tapped to achieve maximum output. Samples from stages 1 and 2 of TSI were rinsed with small known quantities of methanol and made up to 20 and 25 ml respectively with deionized water. The amount of rifampicin deposited in each stage and that remaining in the nebulizer was determined using UV-VIS spectrophotometer (Jenway UV/Vis Spectrophotometer, Staffordshire, UK). The aerodynamic behavior of the nanoparticle suspension was evaluated by calculating nebulization efficiency (NE) and fine particle fraction (FPF) using Eqs. 5 and 6 (8,24). The effective size cut-off between stages for the TSI is 6.4 µm; thus, drug deposited in stage 2 is the fine particle dose (FPD) and the proportion of aerosol generated aerosol deposited in stage 2 is considered the FPF, representing that proportion of delivered product in nebulized droplets having aerodynamic diameter less than 6.4 µm, and predicted to be likely to deposit in the lower airways. Experiments were performed in triplicate and mean values of each parameter are reported.

$$\text{Nebulization efficiency} = \frac{\text{aerosolized drug mass}}{\text{drug mass loaded in nebulizer}} \times 100 \quad (5)$$

$$\text{Fine particle fraction} = \frac{\text{amount of drug in stage 2}}{\text{amount of drug in stage 1 and 2}} \times 100 \quad (6)$$

In vitro Release Studies

Rifampicin-loaded OC nanoparticles were tested for their ability to release rifampicin from the OC-Rif NPs. *In vitro* release study was carried out in the dark with a

dialysis method using modified release technique (25). Simulated lung fluid (SLF—pH 7.4) with 200 µg/ml of ascorbic acid (to prevent oxidative degradation of rifampicin) was used as the dissolution medium. A known amount of OC-Rif NPs (10 mg) was dispersed in SLF and transferred to dialysis membrane of which one end was previously sealed with dialysis tubing clamp. After complete transfer of the formulation, another end of the dialysis membrane was sealed and placed in a beaker containing 25 ml of SLF as external release media under stirring at 37 °C. At selected time intervals, suitable aliquots were withdrawn from the external medium, diluted as required, and analyzed by HPLC (Agilent Technologies 1200 series) at 335 nm (26). Sink condition was maintained (after withdrawal of aliquot at each time points) by replenishing the same amount of blank media. The experiment was carried out in triplicate and results of the release study were plotted as percent cumulative drug release vs time.

HPLC Analysis. The amount of rifampicin released from OC-Rif NPs was analyzed by HPLC (Agilent Technologies 1200 series) equipped with a UV detector to quantify the amount of rifampicin release. The injection volume was 10 µl. Chromatography was performed with a column (Ascentis C18, 150 × 4.6 mm, 5 µm, Supelco, Sigma-Aldrich, USA). Mobile phase comprised tetrahydrofuran (THF)/phosphate buffer (30/70%) at a flow rate of 1.0 ml/min and a detection wavelength of 335 nm (26). The column temperature was set to 40 °C. The retention time of rifampicin was 3.5 min. A calibration curve of pure rifampicin was prepared at concentrations ranging from 5 to 80 µg/ml and was used for quantification of rifampicin in samples.

Cytotoxicity of Octanoyl Chitosan Derivative on A549 Cells Determined by MTT Assay

The MTT cell proliferation assay for OC was performed using the MTT dye reduction assay according to the method described by Kroll et al. (27). The cytotoxicity profiles of OC were studied in the adenocarcinomic human alveolar basal epithelial cell line (A549) over the period of 48 h. The cells (passage no. 45–49) were cultured in 96-well plates with 100 µl complete medium [RPMI-1640, supplemented with fetal bovine serum (10%, FBS) and antimycotic antibiotic solution (1%)] and incubated at 37 °C (5% CO₂ incubator) for the period of 24 h. Samples (100 µl) were prepared in complete medium and added to the wells in a concentrations ranging from 0 to 5 mg/ml and incubated for a further 48 h. After incubation, 40 µg/ml MTT solution (5 mg/ml in PBS, pH 7.4) was added to each well and the plates were again incubated for 2 h at 37 °C (5% CO₂ incubator). Medium was carefully replaced with 100 µl of DMSO in each well to solubilize formazan crystals and the absorbance was read at 570 nm using an ELISA plate reader (SpectraMAX 190, Molecular Devices). The results from the MTT experiments were graphed as percentage of cell growth in comparison to the control wells containing only the cells in the medium and dimethyl sulfoxide (DMSO, 10%) as a positive

control. The relative cell viability (%) was calculated using the following equation:

$$\text{Cell viability (\%)} = \frac{\text{OD of test well}}{\text{OD of reference well}} \times 100$$

Stability Study

Lyophilized OC-Rif NPs were stored in desiccator for 2 months at ambient room temperature (20–25 °C) to determine their stability. After 2 months storage, samples (2 mg) were taken to determine particle size and percentage of rifampicin in the formulation (OC-Rif NPs).

Statistical Analysis

Experiments were performed in triplicate and the data collected are expressed as the mean value ± standard deviation. Results of the factorial design were statistically analyzed using ANOVA (Microsoft Excel Corp, India) and Statistica (Stat soft Inc., Tulsa, USA) by generating various polynomial equations.

RESULTS AND DISCUSSION

Preparation of Nanoparticles and Characterization

Chitosan nanoparticles have previously been prepared using many methods such as ionic gelation, complex coacervation, emulsion cross-linking, and spray drying (28). In addition, polymeric micelles (amphiphilic, self-assembly) prepared using modified chitosan derivatives have also been explored for drug delivery (12,29–31). However, there are no reports of the preparation of nanoparticles directly from hydrophobic chitosan derivatives (OC) using the double emulsion solvent evaporation (DESE) technique without cross-linking. Hence, the current investigation assessed the feasibility of using OC in the preparation of nanoparticles (NPs) and examined the incorporation of rifampicin into OC NPs as a system for the potential treatment of TB via pulmonary route. The DESE method was successfully utilized for the preparation of NPs from OC. Initially, blank OC NPs were prepared and preliminary experiments helped to select optimal parameters such as sonication time, solvent, surfactant, and concentration of surfactant (results are given in supporting information). Once the preliminary parameters were chosen, rifampicin-loaded OC NPs were prepared and optimized employing a 3² factorial design.

Optimization of Formulation by Factorial Design

Based on the preliminary formulation optimization studies, various process parameters required for preparation of OC NPs were selected, which helped to avoid the complexity of experimental design. Thus, optimized parameters such as organic phase (DCM—3.5 ml); internal aqueous phase (0.5 ml); external aqueous phase (10 ml, 0.5% PVA); sonication pulse (15 W); and sonication times of 15 and 30 s for primary and secondary emulsion respectively were kept constant in factorial design studies. Influence of parameters

such as concentrations of OC (X_1) and rifampicin (X_2) were optimized by applying a 3^2 factorial design of experiment consisting of nine formulation batches with random variation of rifampicin and OC at three levels. Table II shows the combination of independent variables and observed responses in terms of mean particle size, entrapment efficiency, and other parameters (PDI, zeta potential, yield and drug loading, etc.) for all the nine formulations.

Effect of Formulation Variables on the Response Parameters

Nine formulations of OC-Rif nanoparticles were prepared according to the 3^2 factorial design and correlation between independent factors and their response parameters in terms of MPS and EE was statistically analyzed using ANOVA (Microsoft Excel Corp, India) and Statistica Stat soft Inc. (Tulsa, USA) by generating various polynomial equations, response surface and contour plots. The data analyzed from the software show the effects of variables on the respective response parameters (Y1 and Y2).

Results of response variables obtained from design of experiment (DoE) were fitted in a simple linear equation, interactive equation or quadratic model equation (Eqs. 8, 9, and 10 respectively) using multiple regression analysis and F-statistic to determine statistically significant terms.

$$Y = \frac{1}{4} (b_0 + b_1X_1 + b_2X_2) \quad \delta 8p$$

$$Y = \frac{1}{4} (b_0 + b_1X_1 + b_2X_2 + b_{12}X_1X_2) \quad \delta 9p$$

$$Y = \frac{1}{4} (b_0 + b_1X_1 + b_2X_2 + b_{11}X_{11} + b_{22}X_{22} + b_{12}X_1X_2) \quad \delta 10p$$

Multiple regressions analysis revealed no significant influence of factors X_1 , X_2 , and X_{22} on the response parameter MPS, while factors X_2 and X_{22} were found to be statistically significant ($p < 0.05$) for % EE. The multiple regression analysis suggested quadratic models as shown in Eqs. 11 and 12 for both MPS and EE respectively. The observed and predicted values of MPS and EE for all the batches of OC-Rif NPs are tabulated in Table III along with their percent relative error (%RE) values as calculated using Eq. 13.

$$Y_1 = \frac{1}{4} (217.71 + 24.89 X_1 + 16.91 X_2 + 37.11 X_{22} + 11.44 X_1X_2) \quad \delta 11p$$

$$Y_2 = \frac{1}{4} (23.81 - 1.32 X_1 + 12.76 X_2 + 4.97 X_{11} + 20.08 X_{22} - 2.48 X_1X_2) \quad \delta 12p$$

$$\% \text{Relative error } \delta RE = \frac{1}{4} \left(\frac{\text{observed Ps} - \text{predicted Ps}}{\text{predicted Ps}} \right) \times 100 \quad \delta 13p$$

Regression output and full model responses for dependent variables, namely MPS and EE of formulation OC-Rif

NPs are displayed in Table IV. The MPS and EE observed after random combinations of three levels of two independent variables (X_1 and X_2) were subjected to multiple regression analysis which revealed statistical significance ($p < 0.05$) of the full model second-order polynomial equation for MPS and EE. In a multiple regression analysis, values of p probability $> F$ less than 0.05 indicate that model terms are significant. In this experiment, analysis of the full model polynomial equation showed p probability $< F$ (0.012), and hence model terms are significant (Eqs. 10 and 11).

The F values for MPS and EE obtained by full model were found to be 25.33 and 45.33 respectively, while corresponding calculated F values (F_{cal}) were 0.34 and 0.11 ($p > 0.05$) respectively, indicating significance ($p > 0.05$). In addition, the goodness of fit of the model was established using the correlation coefficient (R (2)). The correlation coefficient (R^2) values of MPS (0.98) and EE (0.99) showed the total variability in the model. The value of adjusted correlation coefficient (adj R^2) for MPS was found to be 0.9383, whereas 0.9652 for EE as obtained from the full model regression analysis. The predicted R^2 values of MPS and EE were found to be in reasonable agreement with the adj R^2 values, suggesting statistical significance of the model (R^2 value very close to 1), demonstrating very good correlation between the independent variables. Thus, closeness of R^2 values to 1 for both MPS and EE indicated accuracy of the model. Moreover, values of p probability $> F$ were greatly less than 0.05, implying that the model's terms viz. concentration of OC and Rif are statistically significant (p value < 0.05). Together, all of the above considerations indicate that the model can effectively explain 99% variation around the mean value.

It was observed that, the MPS values ranged from 208.17 ± 26.81 nm to 323.57 ± 65.80 nm and entrapment efficiency (EE) of Rif in OC NPs was between $25.4 \pm 3.77\%$ and $64.86 \pm 7.73\%$. A considerably higher entrapment of rifampicin ($64.86 \pm 7.73\%$) was achieved at low levels (-1) of X_1 (50 mg) and high level of X_2 (15 mg) from batch C3. Equations 10 and 11 display the quantitative effect of formulation components (independent variables X_1 and X_2) on response parameters (Y1 and Y2), in the form of corresponding polynomial equations and regression coefficients for mean particle size (MPS—Y1) and mean % entrapment efficiency (EE—Y2).

Each coefficient in equations 10 and 11 was evaluated and the significance determined on the basis of the p values, as shown in Table IV. The smaller the p value ($p < 0.05$), the more statistically significant is the corresponding coefficient. The data obtained from the full model of MPS confirms that the main effects of the independent variables (X_1 , X_2 , and X_{22}) were statistically significant for prediction of MPS as their p values were well below 0.05 ($p < 0.05$), while the interaction term X_1X_2 had little predictive effect as their p values were above 0.05 ($p > 0.05$) and hence were excluded from the model. From the results of EE, p values below 0.05 ($p < 0.05$) were noted for the independent variables X_2 , X_{22} suggesting their statistical significance. Remaining factors such as X_1 , X_{11} and the interaction term X_1X_2 had p values ($p > 0.05$), and therefore they were considered less important in the given model.

The coefficients of the two independent variables in quadratic Eq. 10 were compared and the coefficient value for

Table II. Response Parameters for NPs Prepared Using 3² Factorial Design

Batch	OC (mg)	Rif (mg)	MPS (Y1) (nm)	PDI	ZP (mV)	Yield (%)	DL (%)	EE (Y2) (%)
C1	50	5	242.8 ± 44.36	0.300 ± 0.08	18.83 ± 8.44	60.79 ± 1.43	2.88 ± 0.66	36.83 ± 9.35
C2	50	10	214.4 ± 26.58	0.292 ± 0.04	20.57 ± 8.17	59.88 ± 1.93	4.37 ± 0.18	28.77 ± 0.44
C3	50	15	253.43 ± 19.06	0.323 ± 0.06	23.33 ± 2.83	62.49 ± 3.63	13.51 ± 0.81	64.86 ± 7.73
C4	75	5	242.37 ± 55.54	0.536 ± 0.27	28.8 ± 3.13	65.31 ± 4.73	1.64 ± 0.16	27.87 ± 4.46
C5	75	10	208.17 ± 26.81	0.426 ± 0.14	29.03 ± 13.27	64.84 ± 4.55	2.89 ± 0.26	25.4 ± 3.77
C6	75	15	276.8 ± 58.58	0.327 ± 0.11	25 ± 3.035	65.24 ± 4.24	9.58 ± 1.03	58.33 ± 7.27
C7	100	5	267.2 ± 24.98	0.482 ± 0.03	35.9 ± 2.066	69.29 ± 2.40	1.79 ± 0.13	38.62 ± 4.06
C8	100	10	269.2 ± 107.55	0.447 ± 0.04	31.67 ± 1.79	68.10 ± 1.71	2.49 ± 0.03	27.21 ± 0.94
C9	100	15	323.57 ± 65.80	0.413 ± 0.19	27.3 ± 6.49	68.55 ± 2.46	7.52 ± 0.02	56.72 ± 2.04

$n = 3$; mean ± Standard Deviation

OC—octanoyl chitosan; Rif—rifampicin; MPS—mean particle size; PDI—polydispersity index; EE—entrapment efficiency; DL—drug loading; ZP—zeta potential.

X_1 ($b_1 = 24.89$) was found to be maximum suggesting it was the major contributing factor which affects the mean particle size of OC-Rif NPs. On the other hand, quadratic Eq. 11 showed maximum coefficient values for independent variable X_2 ($b_1 = 12.76$), and hence it was the major factor affecting EE. In both cases, positive values of X_1 and X_2 are an indication of synergistic effect of OC and rifampicin concentration on MPS and EE. Significance of quadratic model terms X_1 and X_2 in Eq. 10 (MPS), and significance of quadratic terms X_2 and X_{22} in Eq. 11 (EE) suggested non-linearity (non-significant) in the ability of independent variables (X_1 and X_2) to influence MPS and EE respectively. The combined effect of factors X_1 and X_2 can be further elucidated with the help of contour plots and response surface curves as shown in Figs. 1a, b and 2a, b.

The predicted residual sum of squares (PRESS) is also known as sum of squared residuals (SSR) or the sum of squared errors of prediction (SSE). PRESS values indicate how well the model fits the data, and it is recommended that, for the chosen model the value of PRESS should be relatively small as compared to the other models under consideration (32). The polynomial model which shows lower PRESS value determines the fitness of data, and hence such model is selected. In the given experiment, PRESS value was calculated for the full and reduced polynomial model for both the

independent variables (Y1 and Y2). Results indicated the suitability of the full polynomial model as compared to the reduced model, with smaller PRESS values for both Y1 (223.96) and Y2 (24.73), whereas the reduced model showed higher PRESS values for Y1 (1493.53) and Y2 (109.17).

Figures 1a, b and 2a, b show contour plots and 3D response surface plots for both response parameters; MPS and EE respectively, depicting the effects of independent variables X_1 and X_2 on dependent variables Y1 and Y2. No significant difference in the MPS and EE was noted, when the value of X_1 was varied from low (− 1) to high (+ 1) level, keeping X_2 constant at low level (− 1). In the similar set up of experiment, when the value of X_2 was increased from low level (− 1) to medium level (0), a non-significant decrease in the particle size was noted which also led to corresponding nonsignificant decrease in the % EE. Further increase in the concentration of X_2 significantly increased EE, while a nonsignificant increase of MPS was observed. Comparing MPS, it was observed that small MPS values in the range of 208.17 ± 26.81 to 323.57 ± 65.80 nm were obtained from all the batches (C1 to C9), with smallest MPS obtained at medium level of X_1 and X_2 from batch C5. The same batch demonstrated the smallest EE (25.4 ± 3.77%). In a different combination, where values of X_2 were increased from low (− 1) to high (+ 1) level and X_1 kept constant at low level

Table III. Observed and Predicted Values of Response Parameter—MPS (Y1); EE (Y2)

Batch	Predicted Y1	Observed Y1	Residual Y1	%RE Y1	Predicted Y2	Observed Y2	Residual Y2	%RE Y2
C1	243.78	242.80 ± 44.36	− 0.975	− 0.399	34.93	36.83 ± 9.35	1.89	5.43
C2	212.14	214.40 ± 26.58	2.26	1.065	30.09	28.77 ± 0.44	− 1.33	− 4.41
C3	254.72	253.43 ± 19.06	− 1.285	− 0.504	65.43	64.86 ± 7.73	− 0.57	− 0.87
C4	237.91	242.37 ± 55.54	4.46	1.875	31.13	27.87 ± 4.46	− 3.26	− 10.46
C5	217.71	208.17 ± 26.81	− 9.54	− 4.382	23.81	25.40 ± 3.77	1.58	6.65
C6	271.72	276.80 ± 58.58	5.08	1.869	56.66	58.33 ± 7.27	1.67	2.95
C7	270.69	267.20 ± 24.98	− 3.485	− 1.288	37.26	38.62 ± 4.062	1.36	3.65
C8	261.92	269.20 ± 107.55	7.28	2.779	27.46	27.21 ± 0.94	− 0.26	− 0.93
C9	327.37	323.57 ± 65.80	− 3.795	− 1.159	57.83	56.72 ± 2.037	− 1.10	− 1.91

$n = 3$, mean ± SD

MPS—mean particle size; EE—entrapment efficiency

Table IV. Response of Full Model of OC-Rif NPs

	MPS		EE	
	Coefficients	<i>p</i> value	Coefficients	<i>p</i> value
X1	24.890	0.0059*	- 1.317	0.343
X2	16.905	0.0173*	12.76	0.002*
X11	19.320	0.0508	4.969	0.092
X22	37.105	0.0089*	20.08	0.002*
X1X2	11.435	0.0772	- 2.482	0.1823
Intercept	217.71	5.69E-05#	23.81	0.0016#

*Statistically significant (*p* < 0.05)

Significance of *F* value

MPS—mean particle size; EE—entrapment efficiency

(- 1), results showed non-significant decrease in value of MPS (214.4 ± 26.58 nm) initially at the medium level of X₁ (0), which further increased (253.43 ± 19.06 nm) at high level (+ 1) of X₁. Entrapment efficiency also showed similar trend (28.77 ± 0.44% (X₁ - 0) and 64.86 ± 7.73% (X₁ + 1)) with increased concentration of Rif. Among all the batches tested, optimum MPS with maximum EE was obtained with batch C3, formulated with the combination of low level of X₁ (50 mg) and high (+ 1) level of X₂ (15 mg). The results can be observed from the contour plots and 3D response surface plot as displayed in Figs. 1a, b and 2a, b. The predicted and observed values of response parameter (MPS and EE) are shown in Table III. Low percent relative error values (below 10%) and small residuals were demonstrated by the full polynomial model of MPS and EE (Table IV), confirming the reasonable agreement between predicted and experimental values and indicated suitability of the model. ANOVA full model results of MPS and EE are given in Table V.

Effect of Polymer Concentration and Theoretical Drug Loading on MPS, EE, and ZP

A non-significant influence of theoretical drug loading (DL) on MPS was observed at all levels. Theoretical DL of 5,

10, and 15 mg of rifampicin resulted in MPS of 242.8 ± 44.36, 214.4 ± 26.58, and 253.43 ± 19.06 nm respectively. Similar results were obtained even when the concentration of polymer was increased from 50 to 75 and 100 mg. Such a relation between the theoretical DL and polymer concentration on MPS was also observed by Doan et al. (33). Although MPS from all the batches were obtained in the range of 208.17 ± 26.81 to 323.57 ± 65.80 nm, larger MPS was observed when the concentration of polymer and drug was increased. Formulation C1–C3 consisting of lowest concentration of OC (50 mg) and varying amounts of Rif (5–15 mg) showed lowest values of PDI (0.292 ± 0.036 to 0.323 ± 0.059), whereas increasing concentration of OC to 75 and 100 mg led to increase in the PDI values suggesting broader particle distributions (PDI > 0.4). Non-significant increases in the MPS (276.8 ± 58.58 nm and 323.57 ± 65.80 nm with PDI of 0.427 ± 0.107 and 0.413 ± 0.188) with increased amount of OC (75 and 100 mg) may be due to an increase in the viscosity of the organic phase in the emulsion, which might have caused hindrance in the efficiency of sonication. Reports have also suggested possible collision and merger of nanoparticles leading to large MPS, when higher polymer concentration was used for the preparation of NPs (34,35). Based on the results of this study, batch C3 composed of 50 mg of polymer and 15 mg of Rif exhibited optimum particle size with uniform size distribution as compared to other batches prepared with other combinations of OC-Rif concentration.

Factorial design of experiment yielded formulation batches with the variable entrapment efficiencies of Rif in OC. At low polymer concentration (50 mg), the highest entrapment efficiency (64.86 ± 7.73%) was obtained, when the theoretical DL was kept at a higher level of 15 mg (batch C3). Similar pattern of results in terms of increased EE was observed when the amount of OC was increased to 75 and 100 mg in batch C6 and C9 with the corresponding EE of 58.33 ± 7.27 and 56.72 ± 2.037% respectively. The use of the highest OC concentration (100 mg) for the preparation of NPs led to non-significant decrease in the EE, which may be due to enhanced viscosity of the system contributing to hampered sonication and stirring (36). Considerably lower EEs of 36.83 ± 9.35% and 28.77 ± 0.44% were noted at lower theoretical DL of 5 and 10 mg

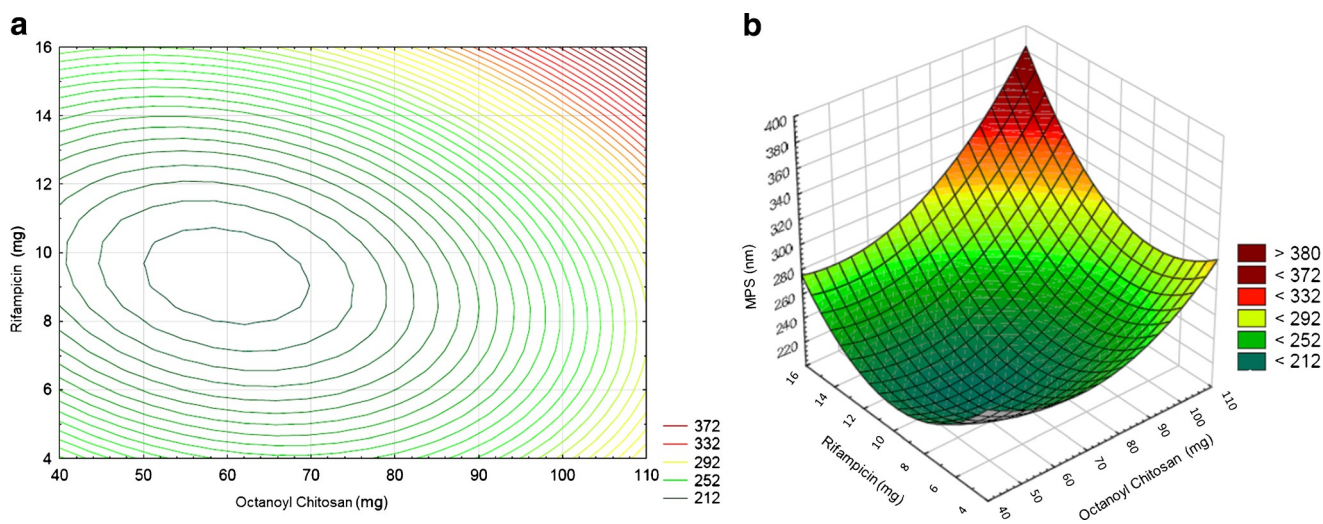


Fig. 1. a Contour plot showing the effect of independent factors on mean particle size (MPS). b Response surface plot showing the effect of independent factors on MPS

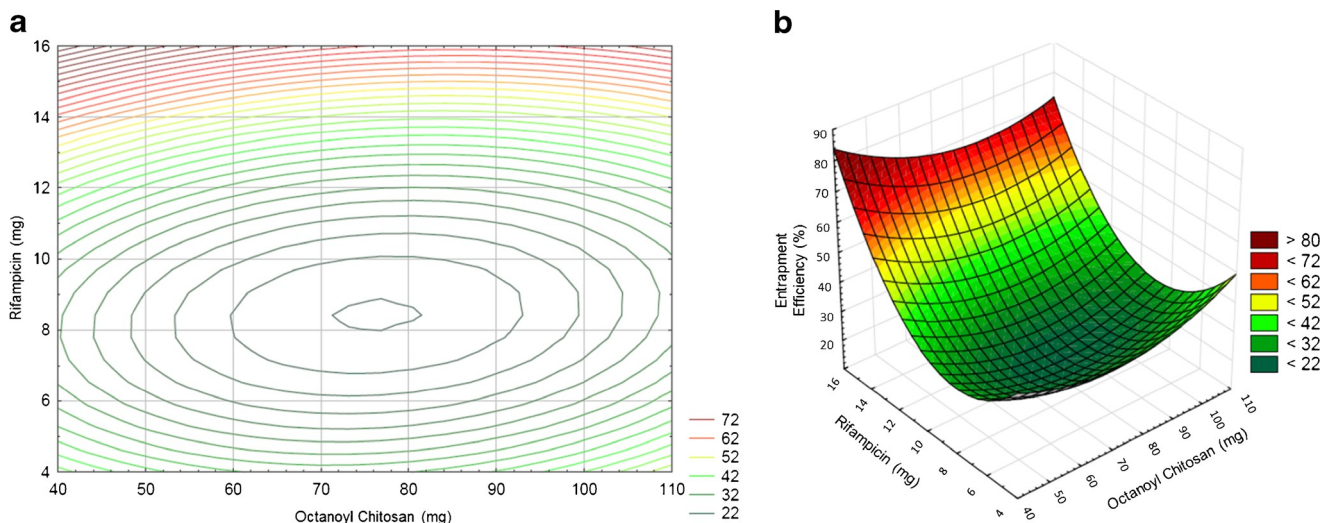


Fig. 2. a Contour plot showing the effect of independent factors on entrapment efficiency (EE). b Contour plot showing the effect of independent factors on EE

respectively. The same trend was noted in all the batches studied. Thus, a non-significant change in the entrapment efficiency was observed at low and medium theoretical drug loading at all polymer concentrations, while high theoretical drug loading showed increased entrapment efficiency, which may be due to higher amount of drug available for entrapment. (37,38) Similar results have been reported previously (39,40). Other studies have also reported increased theoretical DL associated with increased EE and size (41,42). PDI relates to the distribution of particle sizes in a sample of particles. Smaller PDI values close to 0 are preferred, indicating a narrow size distribution (43). Results of this study demonstrated acceptable PDI values at low polymer concentration, while higher PDI values (> 0.4) were observed for the batches prepared using higher amounts of OC (Table II).

A positive zeta potential conferred by the polymers is usually preferred in the delivery of small molecules and macromolecules due to advantages such as ease in surface assimilation of negatively charged materials such pDNA and RNA, drugs, and even proteins, and their ability to interact with cells thereby providing high transfection efficiency (44). Moreover, cationic polymers have also been explored for the purification of water (45). The current investigation was directed to modify chitosan

while retaining its positive charge. All the batches from C1 to C9 showed positive ZP ranging from + 18.83 ± 8.44 to + 35.90 ± 2.07 mV. Although no correlation between charge on the particles and amount of drug was seen, increasing the polymer concentration had a positive influence on the charge. This enhancement in the ZP can be rated as C1 < C4 < C7 (+ 18.83 ± 8.44 < + 28.8 ± 3.13 < + 35.90 ± 2.07 mV) and C2 < C5 < C8 and C3 < C6 < C9, with respect to increase in polymer concentration. Increased ZP values for rifampicin-loaded OC NPs, as compared to their blank counterparts were observed. This increased ZP could be attributed to the particle-associated rifampicin (adsorbed), which might have influenced surface charge owing to the presence of amino groups in the rifampicin molecule (46).

Optimization of Responses Using Desirability Function (47)

The difficulty of multiple and sometimes opposing responses is usually overcome by an optimization technique involving desirability function. Each response is affiliated with its own partial desirability function. The value of 1 for the desirability function is always preferred as it is considered optimal, while value of zero means the result is treated unacceptable. The desirability for each response can be calculated at a given response point in the experimental design. When the goal is to minimize the given response, the following formula can be used to calculate individual desirability.

Table V. Analysis of Variance (ANOVA) of MPS and EE for Full Models of OC-Rif NPs

Results of MPS						
	df	SS	MS	F	R ²	Adj R ²
Regression	5	9454.87	1890.97	25.33	0.98	0.94
Residual	3	223.96	74.65	-	-	-
Total	8	9678.83	-	-	-	-
Results of EE						
	df	SS	MS	F	R ²	Adj R ²
Regression	5	1868.55	373.71	45.33	0.99	0.97
Residual	3	24.73	8.24	-	-	-
Total	8	1893.28	-	-	-	-

df—degrees of freedom; SS—sum of squares; MS—mean of squares; F Fischer's ratio; R² regression coefficient; MPS—mean particle size; EE—entrapment efficiency

$$d_i = \frac{Y_i - U_i}{T_i - U_i} \quad (14)$$

where d_i is individual desirability, Y_i (mps) is experimental results of response MPS. U_i and T_i stand for maximum and target MPS respectively. Similarly, if one wants to maximize the stated response, Eq. 15 can be used to calculate individual desirability.

$$d_i = \frac{Y_i - L_i}{T_i - L_i} \quad (15)$$

where d_i is individual desirability, Y_i (e) is experimental results of response MPS. T_i and L_i stand for minimum and target EE respectively. Once we get this, we can calculate combined desirability (D) using Eq.16, which involves multiplication of individual desirability.

$$D = \sqrt[k]{d_1 \times d_2 \times \dots \times d_k}$$

where, k denotes total number of responses.

Optimum parameters for the formulation were generated utilizing a numerical optimization technique by the desirability function approach. Response parameters such as Y_1 and Y_2 were optimized and the optimized formula was finalized by keeping the mean particle diameter in the range 200 to 300 nm and EE between 50 and 70%. Batch C3 (containing low (-1) level of variable X_1 and high level of variable X_2) resulted in the optimum formula. Individual desirability for MPS and EE was calculated and found to be 1, indicating acceptability of the model for the optimization of formula. Similarly, overall desirability for the current model was also found to be 1, indicating suitability of the model for optimization purposes. Moreover, the result of the experimental and predicted values for MPS and EE confirmed the practicability and validity of the model. Relative errors for both MPS and EE were found to be below 10% indicating that the response surface methodology (RSM) optimization technique was appropriate for optimization for the preparation of NPs from the novel polymer and for incorporation of Rif in OCNPs.

Optimized Formulation

The rigorous optimization process yielded a final formula (Table VI), which was used in further studies. Table VI also shows the predicted and observed values of various parameters.

Lyophilization of OC-Rif NPs was done in the presence of trehalose as a cryoprotective agent at a concentration of 1% (20). Almost comparable results with respect to mean particle size were achieved in the samples before (231.9 ± 20.37) and after lyophilization (253.43 ± 19.06 nm), with no significant change in mean size following lyophilization ($P > 0.05$). This has indicated the suitability of trehalose (1%) as a cryoprotectant during lyophilization.

Particle Characterization

Particle Size and Surface Charge

OC-Rif NPs prepared using the optimized final formula were centrifuged and washed to remove any untrapped materials (Rif and PVA) and mean hydrodynamic diameter, PDI, and zeta potential were determined prior to freeze drying (FD). The preparation had mean particle size of 231.9 ± 20.37 nm, PDI of 0.384 ± 0.022 , and ZP of $+28.2 \pm 1.67$ mV. After redispersion of freeze-dried OC-Rif-NP powder, the measured values for MPS, PDI, and ZP were very similar (Table VI).

Morphology of OC-Rif NPs After Freeze Drying

The size, shape, and surface morphology of nanoparticles were visualized by scanning and transmission electron microscopy (SEM and TEM) (Fig. 3a, b) respectively. OC-Rif NPs were uniform in size and morphology, showed small particle diameter, spherical shape, and smooth surface morphology.

Solid-State Characterization of OC-Rif NPs

Differential Scanning Calorimeter

Thermal analysis of rifampicin, OC, OC-Rif physical mixture and OC-Rif NPs formulation was performed using DSC and the data obtained in the form of thermograms are presented in Fig. 4. Thermograms revealed a characteristic exothermic peak at 260°C for rifampicin with no endothermic and exothermic peak between 20 to 300°C in the thermogram of OC. However, an exothermic peak was observed above 300°C in the thermogram of chitosan, which is attributed to monomer dehydration, glycoside bond cleavage and decomposition of the acetyl and deacetylated units of chitosan. Similar results have been reported previously (48,49). Similarly, physical mixture of OC and rifampicin did not show any endothermic or exothermic peak for OC, but an exothermic peak corresponding to rifampicin was observed at 260°C . Owing to the absence of endothermic or exothermic peak in OC thermograms, DSC thermographs of OC-Rif NPs formulation were also devoid of endothermic or exothermic peaks. In addition, the absence of a peak for rifampicin in the OC-Rif NPs suggested molecular dispersion of rifampicin in OC NPs.

Table VI. Optimized Formulation Parameters; Observed and Predicted Values for OC-Rif NPs

Formulation parameters	Optimum value	Parameters	Y1 (nm)	Y2 (%)
OC (mg)	50	Predicted	254.72	65.43
Vol. of organic phase (ml)	3.5	Observed	253.43 ± 19.06	64.86 ± 7.73
Rifampicin content (mg)	15	% RE	0.504	0.87
Vol. of internal aqueous Phase (ml)	0.5	Residuals	-1.285	-0.57
Surfactant in external aqueous phase	PVA	ZP observed	$+23.33 \pm 2.83$	
Concentration of surfactant in external aqueous phase (% w/v)	0.5			
Vol. of external aqueous phase (ml)	10			

OC—octanoyl chitosan; PVA—polyvinyl alcohol

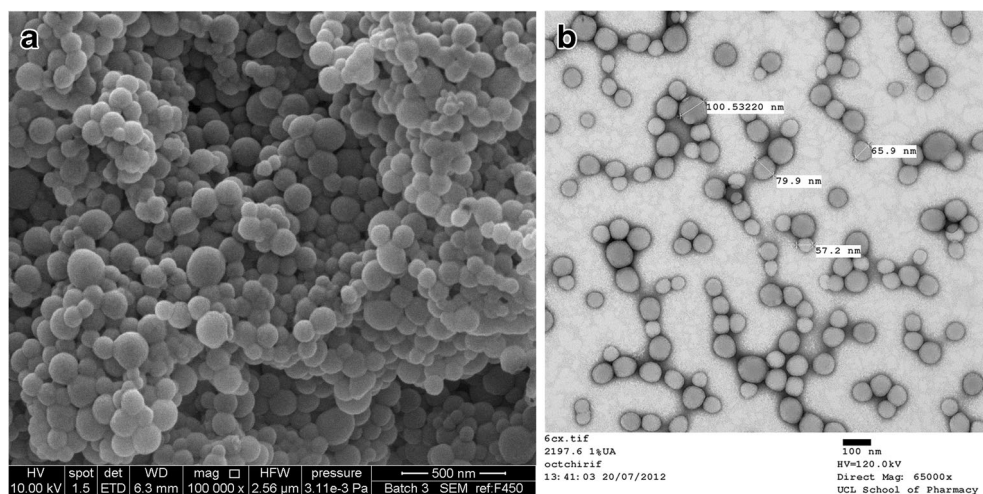


Fig. 3. a Scanning electron micrograph of OC-Rif NPs. b Transmission electron micrograph of OC-Rif NPs

X-ray Powder Diffraction

X-ray diffractograms of rifampicin, chitosan, OC, and OC-Rif NPs are shown in Fig. 5. Characteristic crystalline peaks at 2θ values of 13° and 15° for rifampicin were observed in the powder XRD diffractograms. XRD of Rif indicated the crystalline nature of rifampicin. Parent chitosan (chitosan > 5 K) showed a characteristic broad peak of moderately low intensity at around 20° , whereas a sharp

peak at 20° and a new peak of higher intensity below 2θ value of 8 were observed in the XRD spectra of OC. XRD studies revealed a broad diffuse peak for rifampicin-loaded NPs (OC-Rif NPs). The absence of crystalline peak of rifampicin in the OC-Rif NPs suggested the presence of rifampicin in amorphous form in OC NPs and its molecular dispersion in OC NPs. Presence of a broad diffuse peak in XRD diffractograms of rifampicin-loaded OC NPs is a general characteristic for such systems composed of binary components (50). Results from XRD have demonstrated that crystallinity of rifampicin was altered by its encapsulation into OC nanoparticle formulation.

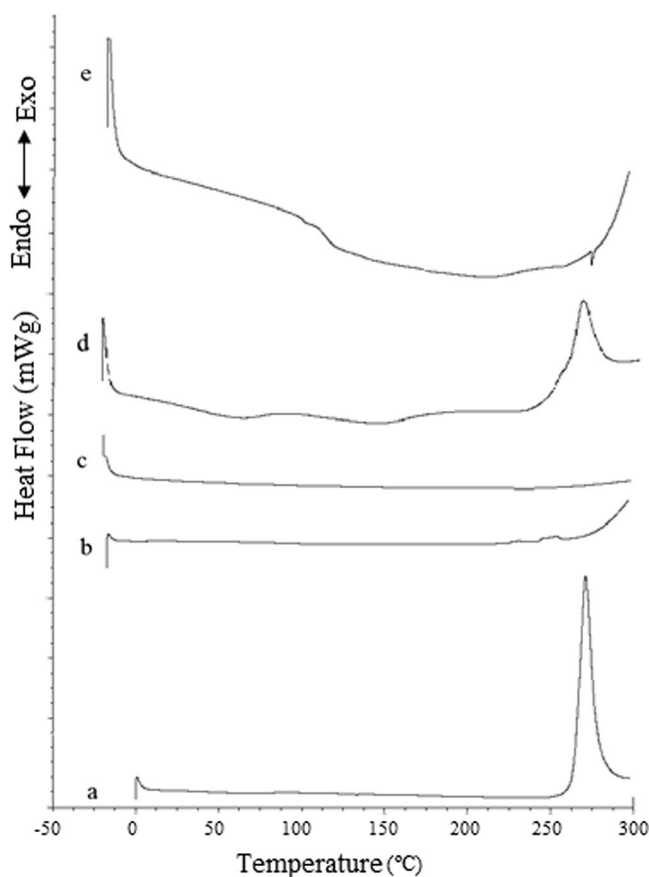


Fig. 4. DSC thermograms of a Rif, b Chitosan, c OC, d OC-Rif physical mixture, and e OC-Rif NPs

Aerosol Characterization Using the Twin-Stage Impinger

Samples for TSI studies were prepared by dispersing 10 mg of OC-Rif NPs in 5 ml deionized water and nebulized using a PariBoy air-jet nebulizer into the TSI (Table VII).

Following nebulization to dryness 0.45 ± 0.06 mg of Rif was deposited in stage 2 of the TSI (*i.e.* the FPD) representing an FPF of $43.27 \pm 4.24\%$. The amount of drug remaining in the nebulizer, caused by the residual volume (51) of the nebulizer was found to be 0.59 ± 0.06 mg giving a nebulizer efficiency of $77.04 \pm 4.33\%$.

These findings indicate the suitability of the jet nebulizer to deliver rifampicin, in a mucoadhesive NP carrier system to the lower respiratory tract. Such nebulizers have previously been reported to achieve efficient aerosolization of nanocarriers (6,52), with the small particles being efficiently delivered in the relatively large nebulized aerosol droplets which are efficiently delivered to the lower stage of the TSI and human lower respiratory tract.

In vitro Drug Release

The cumulative percentage release of Rif from Rifampicin suspension (Rif-S) and OC-Rif NPs was investigated *in vitro* over a period of 2 h and 72 h respectively. Experiment was performed in triplicate and release curves plotted as cumulative percentage drug release vs time are shown in Fig. 6. Simulated lung fluid (SLF 4, pH 7.4) was used as a release medium, to mimic the biological environment within

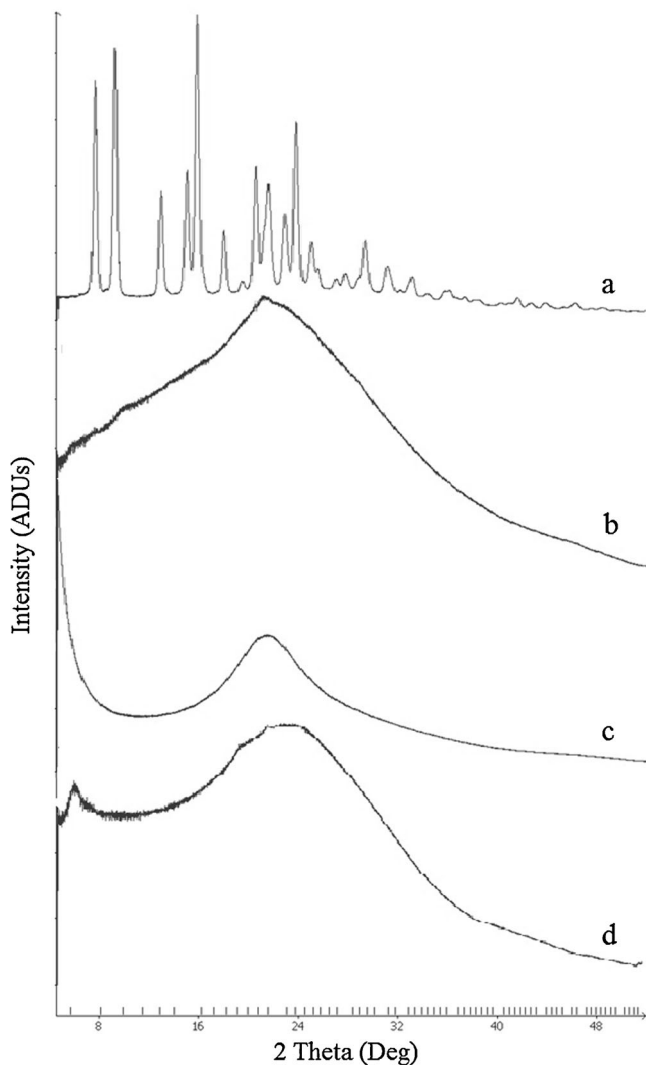


Fig. 5. X-Ray diffractograms of a Rif, b Chitosan, c OC, and d OC-Rif NPs

the lungs into which aerosolized NPs will be deposited. Results showed immediate release of almost all the rifampicin ($87.65 \pm 10.29\%$) from Rif-S into release medium, whereas release of rifampicin was retarded from the OC NPs. OC-Rif NPs displayed initial rifampicin release of $5.23 \pm 3.15\%$, indicating the ability of the polymer matrix to control the release of drug. OC-Rif NPs exhibited sustained and steady release over the period of study (72 h), with a biphasic drug release pattern. Initially, a sustained-release phase was observed until 6 h, which was followed by a steady, slower

drug release. In the initial phase (up to 6 h), $45.97 \pm 2.99\%$ of rifampicin release was noted, which may have been due to dissolution and passive diffusion of Rif located on or near the surface of nanoparticles. In addition, penetration of aqueous release medium (SLF pH 7.4) into the hydrophobic polymeric matrix leading to slow dissolution and thereby diffusion of the drug from the OC NP matrix may also have caused sustained initial release up to 6 h. After 6 h, a slower release of drug occurred, leading to loss of $73.14 \pm 3.17\%$ of drug at 72 h. The second phase of drug release is probably due to the diminution of rifampicin in the polymeric matrix, leading to a reduced concentration gradient, causing less drug to be released. Hence, the biphasic release pattern of the formulation can be ascribed to the localization of rifampicin onto and within the immediate layer and core of the prepared nanoparticles. These results agree with the observations described by Klariæ et al. (53).

The release profiles obtained were fitted using various mathematical models, namely: zero-order, first-order, Higuchi, Hixon-Crowell, and Korsmeyers-Peppas models to explore the kinetics of drug release from OC nanoparticles (54). The results of different model fittings are given in Fig. 6. Among various models tested, the curve fitting of release data to the Korsmeyers-Peppas model gave a higher value of correlation coefficient (r^2 value of 0.8243) with the bn^{\wedge} value (0.911, which is $0.5 < n < 1$), suggesting an anomalous transport (non-fickian) mechanism for rifampicin release. Thus, the Korsmeyers-Peppas model satisfactorily represented the data owing to diffusion of rifampicin from the OC NPs.

Cytotoxicity Studies of OC

A very important criterion determining the suitability of polymers in drug delivery is their cytotoxicity. Non-cytotoxic materials are always preferred while choosing carrier materials for drug delivery. Cationic agents are reported usually to confer cytotoxicity owing to their interaction with negatively charged cellular elements or proteins (55). However, chitosan and its derivatives are described as less cytotoxic than other cationic polymers (for instance poly-lysine and polyethyleneimine) (56). The cytotoxicity caused by chitosan and its derivative is mainly determined by the factors such as type of chitosan derivative and type of cells under study (54). This study used chitosan derivatives and tested the viability of cells treated with OC by application of the MTT assay (Fig. 7). Results indicated non-significant changes in the cell viability at the examined concentrations of OC in comparison to the controls (positive and negative), demonstrating *in vitro* biocompatibility of OC over the concentration range studied.

Table VII. Aerosol Properties of Nebulized of OC-Rif NPs Measured Using TSI

Batch	Dose filled in nebulizer (mg)	FPD (mg)	Dose remained in nebulizer (mg)	NE %	FPF (%)
Batch C3 (OC-Rif NPs)	1.35	0.45 ± 0.06	0.59 ± 0.06	77.04 ± 4.33	43.27 ± 4.24

$n = 3$, mean \pm SD

NE—nebulization efficiency; FPF—fine particle fraction; FPD—fine particle dose

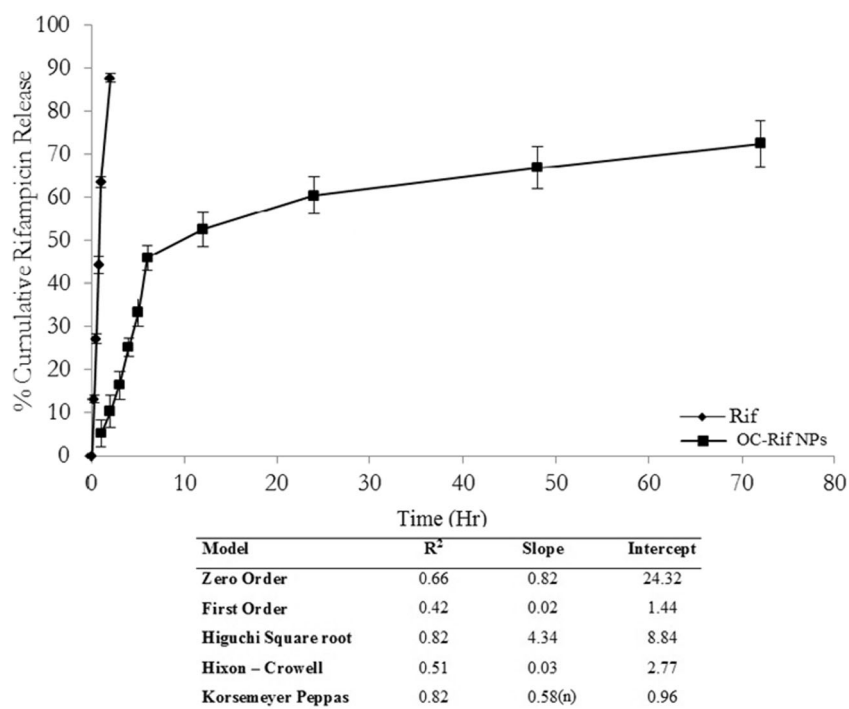


Fig. 6. Percent cumulative release of Rif from OC-Rif nanoparticles ($n= 3$, mean \pm SD)

Stability Studies

OC-Rif NPs were assessed for their ability to maintain their mean particle size and size distribution along with their content of rifampicin over the period of 2 months storage at ambient temperature (Table VIII). No significant differences ($P > 0.05$) were observed for drug content, mean particle size or PDI values of OC-Rif NPs, confirming the stability of OC-Rif NPs at ambient room temperature (20–25 °C). Hence, no special storage conditions were necessary up to 2 months.

CONCLUSIONS

This study has shown that derivatization of chitosan with a hydrophobic octanoyl chain increased the hydrophobicity of the polymer with no cytotoxicity. Octanoyl chitosan was successfully utilized to prepare nanoparticle preparations using double emulsion method, which is frequently used for preparation of nanoparticles. However, chitosan, nanoparticles often have to be hardened by cross-linking with potentially toxic agents. Formulations were optimized by factorial design. The optimized batch, with optimum physico-

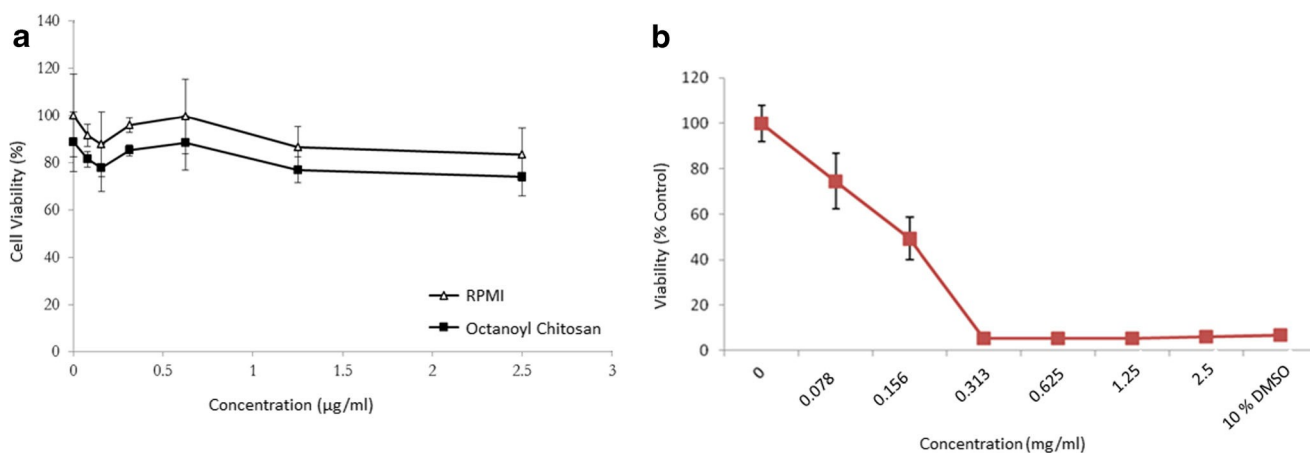


Fig. 7. *In vitro* cytotoxicity of a RPMI control and octanoyl chitosan and b DMSO control in A549 cells. ($n= 3$, mean \pm SD)

Table VIII. Stability of OC-Rif NPs at Ambient RT

Sr. no.	Time (months)	Drug content (%)	MPS (nm)	PDI
1	Initial	100	253.43 ± 19.06	0.323 ± 0.059
2	2	98.03 ± 5.26	261.73 ± 16.37	0.402 ± 0.014

$n = 3$, mean ± SD; MPS—mean particle size, PDI—polydispersity index

chemical parameters exhibited good incorporation of rifampicin in the octanoyl chitosan nanoparticles. Electron microscopy revealed spherical particles with smooth surfaces, while DSC and XRD studies indicated molecular dispersion of rifampicin in the octanoyl chitosan nanoparticles. The sphericity and positive surface charge of the octanoyl chitosan nanocarriers are expected to increase cell surface affinity and uptake of nanocarriers (57). In addition, the mucoadhesive/bioadhesive property of chitosan would potentially increase the residence time of the formulations in the lungs, successfully delivered from a jet nebulizer, which might enhance the efficiency of antibiotic for the treatment of infections. Biodegradability and non-cytotoxicity (as determined by MTT assay) of this natural polymer suggests its likely safety in clinical use. In sum, the results of this study have demonstrated the desirable potential of octanoyl chitosan and octanoyl chitosan nanoparticles for lung delivery of rifampicin. Further evaluations in animals are required to further evaluate its utility and potential clinical use.

ACKNOWLEDGEMENTS

The authors would like to thank Mr. David McCarthy (UCL) for SEM images.

FUNDING INFORMATION

One of the authors, Dr. Kailash C. Petkar would like to thank the Commonwealth Commission, UK, and UCL School of Pharmacy, London, for providing financial assistance.

COMPLIANCE WITH ETHICAL STANDARDS

Conflict of Interest The authors declare there is no conflict of interest.

REFERENCES

- World Health Organization. Global TB control—epidemiology, strategy, financing. Programs and Projects: WHO Global Tuberculosis Report - 2017. 2016. (http://www.who.int/tb/publications/global_report/gtbr2015_executive_summary.pdf?ua=1) (Date accessed Dec. 2017).
- Ishikawaa AA, Salazarb JV, Salinasc M, Gaitania CM, Nurkiewicz T, Negretec GR, et al. Self-assembled nanospheres for encapsulation and aerosolization of rifampicin. *RSC Adv*. 2016;6(16):12959–63.
- Singh C, Koduri LV, Dhawale V, Bhatt TD, Kumar R, Grover V, et al. Potential of aerosolized rifampicin lipospheres for modulation of pulmonary pharmacokinetics and bio-distribution. *Int J Pharm*. 2015;495:627–32.
- Rawal T, Parmar R, Tyagi R, Butani S. Rifampicin loaded chitosan nanoparticle dry powder presents an improved therapeutic approach for alveolar tuberculosis. *Colloids Surf B Biointerfaces*. 2017;154:321–30.
- González-Juarrero M, O'Sullivan MP. Optimization of inhaled therapies for tuberculosis: the role of macrophages and dendritic cells. *Tuberculosis*. 2011;91(1):86–92.
- Mansour HM, Rhee YS, Wu X. Nanomedicine in pulmonary delivery. *Int J Nanomedicine*. 2009;4:299–319.
- Menon JY, Ravikumar P, Pise A, Gyawali D, Hsia CCW, Nguyen KT. Polymeric nanoparticles for pulmonary protein and DNA delivery. *Acta Biomater*. 2014;10:2643–52.
- Efiana NA, Mahmood A, Lam HT, Zupančić O, Leonaviciute G, Bernkop-Schnürch A. Improved mucoadhesive properties of self-nanoemulsifying drug delivery systems (SNEDDS) by introducing acyl chitosan. *Int J Pharm*. 2017;519(1–2):206–12.
- Moschos SA, Bramwell VW, Somavarapu S, Alpar HO. Comparative immunomodulatory properties of a chitosan-MDP adjuvant combination following intranasal or intramuscular immunisation. *Vaccine*. 2005;23(16):1923–30.
- Grenha A, Seijo B, Remuán-López C. Microencapsulated chitosan nanoparticles for lung protein delivery. *Eur J Pharm Sci*. 2005;25(4–5):427–37.
- Li HY, Seville PC. Novel pMDI formulations for pulmonary delivery of proteins. *Int J Pharm*. 2010;385:73–8.
- Amidi M, Romeijn SG, Verhoef JC, Junginger HE, Bungener L, Huckriede A, et al. N-trimethyl chitosan (TMC) nanoparticles loaded with influenza subunit antigen for intranasal vaccination: biological properties and immunogenicity in a mouse model. *Vaccine*. 2007;25(1):144–53.
- Motiei M, Kashanian S. Novel amphiphilic chitosan nanocarriers for sustained oral delivery of hydrophobic drugs. *Eur J Pharm Sci*. 2017;99:285–91.
- Huang Y, Yu H, Guo L, Huang Q. Structure and self-assembly properties of a new chitosan-based amphiphile. *J Phys Chem B*. 2010;114(23):7719–26.
- Mourya VK, Inamdar NN. Chitosan modifications and application: opportunities galore. *React Funct Polym*. 2008;68:1013–51.
- Zhang J, Chen XG, Li YY, Liu CS. Self-assembled nanoparticles based on hydrophobically modified chitosan as carriers for doxorubicin. *Nanomedicine*. 2007;3(4):258–65.
- Cho Y, Kim TJ, Park HJ. Size-controlled self-aggregated N-acyl chitosan nanoparticles as a vitamin C carrier. *Carbohydr Polym*. 2012;88(3):1087–92.
- Cho Y, Kim TJ, Park HJ. Preparation, characterization, and protein loading properties of N-acyl chitosan nanoparticles. *J Appl Polym Sci*. 2012;124:1366–71.
- Pandey R, Sharma A, Zahoor A, Sharma S, Khuller GK, Prasad B. Poly (DL-lactide-co-glycolide) nanoparticle-based inhalable sustained drug delivery system for experimental tuberculosis. *J Antimicrob Chemother*. 2003;52:981–6.
- Holzer M, Vogel V, Mantele W, Schwartz D, Haase W, Langer K. Physico-chemical characterisation of PLGA nanoparticles after freeze-drying and storage. *Eur J Pharm Biopharm*. 2009;72:428–37.
- Bolton S, Charles S. *Pharmaceutical statistics*. New York: Marcel Dekker Inc; 2004. p. 249–55.
- Benetton SA, Kedor-Hackmann ERM, Santoro MIRM, Borges VM. Visible spectrophotometric and first-derivative UV spectrophotometric determination of rifampicin and isoniazid in pharmaceutical preparations. *Talanta*. 1998;47(3):639–43.
- European Directorate for the Quality of Medicines, European Pharmacopoeia 9.0 (Ph. Eur. 9th Edn.), Method Chapter 2.9.18, Preparations for inhalation: aerodynamic assessment of fine particles. 2017. Pg. No. 323 (Strasbourg, Council of Europe).
- Liu J, Gong T, Fu H, Wang C, Wang X, Chena Q, et al. Solid lipid nanoparticles for pulmonary delivery of insulin. *Int J Pharm*. 2008;356:333–44.
- Marques MRC, Loebenberg R, Almukainzi M. Simulated biological fluids with possible application in dissolution testing. *Dissolut Technol*. 2011;18:15–28.

26. Tatarczak M, Flieger J, Szumilo H. High-performance liquid-chromatographic determination of rifampicin in complex pharmaceutical preparation and in serum mycobacterium tuberculosis-infected patients. *Acta Pol Pharm Drug Res.* 2005;62(4):251–6.
27. Kroll A, Dierker C, Rommel C, Hahn D, Wohlleben W, Schulze-Isfort S, et al. Cytotoxicity screening of 23 engineered nanomaterial using a test matrix of ten cell lines and three different assays. *Part Fibre Toxicol.* 2011;8:9.
28. Grenha A. Chitosan nanoparticles: a survey of preparation methods. *J Drug Target.* 2012;20(4):291–300.
29. Aranaz I, Harris R, Heras A. Chitosan amphiphilic derivatives. Chemistry and applications. *Curr Org Chem.* 2010;14:308–30.
30. Li Y, Zhang S, Meng X, Chen X, Ren G. The preparation and characterization of a novel amphiphilic oleoyl-carboxymethyl chitosan self-assembled nanoparticles. *Carbohydr Polym.* 2011;83:130–6.
31. Hu L, Suna Y, Wu Y. Advances in chitosan-based drug delivery vehicles. *Nano.* 2013;5:3103.
32. Shah PP, Mashru RC, Rane YM, Thakkar A. Design and optimization of mefloquine hydrochloride microparticles for bitter taste masking. *AAPS PharmSciTech.* 2008;9(2):377–89.
33. Doan TVP, Couet W, Olivier JC. Formulation and in vitro characterization of inhalable rifampicin-loaded PLGA microspheres for sustained lung delivery. *Int J Pharm.* 2011;414:112–7.
34. Bhavsar MD, Tiwari SB, Amiji MM. Formulation optimization for the nanoparticles-in-microsphere hybrid oral delivery system using factorial design. *J Control Release.* 2006;110(2):422–30.
35. Murakami H, Kobayashi M, Takeuchi H, Kawashima Y. Preparation of poly(DL-lactide-co-glycolide) nanoparticles by modified spontaneous emulsification solvent diffusion method. *Int J Pharm.* 1999;187:143–52.
36. Kirby DJ, Rosenkrands I, Agger EM, Andersen P, Coombes AG, Perrie Y. PLGA microspheres for the delivery of a novel subunit TB vaccine. *J Drug Target.* 2008;16(4):282–93.
37. Bilati U, Allémann, Doelker E. Poly(D,L-lactide-co-glycolide) protein-loaded nanoparticles prepared by the double emulsion method—processing and formulation issues for enhanced entrapment efficiency. *J Microencapsul.* 2009;22(2):205–14.
38. Alex R, Bodmeier R. Encapsulation of water-soluble drugs by a modified solvent evaporation method. I. Effect of process and formulation variables on drug entrapment. *J Microencapsul.* 1990;7:347–55.
39. Conway BR, Alpar HO. Double emulsion microencapsulation of proteins as model antigens using polylactide polymers: effect of emulsifier on the microsphere characteristics and release kinetics. *Eur J Pharm Biopharm.* 1996;42:42–8.
40. Yang YY, Chung TS, Ng N. Morphology, drug distribution, and in vitro release profiles of biodegradable polymeric microspheres containing protein fabricated by double-emulsion solvent extraction/evaporation method. *Biomaterials.* 2011;22:231–41.
41. Atkins TW, Peacock J. The incorporation and release of bovine serum albumin from poly-hydroxybutyratehydroxyvalerate microcapsules. *J Microencapsul.* 1996;13:709–17.
42. Jeffery H, Davis SS, O'Hagan DT. The preparation and characterization of poly(lactide-co-glycolide) microparticles. II. The entrapment of a model protein using a (water-in-oil)-in-water emulsion solvent evaporation technique. *Pharm Res.* 1993;10:362–8.
43. Ranjan AP, Mukerjee A, Helson L, Vishwanatha JK. Scale up, optimization and stability analysis of Curcumin C3 complex-loaded nanoparticles for cancer therapy. *J Nanobiotechnol.* 2012;10:38.
44. Lubben IMV, Verhoef JC, Borchard G, Junginger HE. Chitosan and its derivatives in mucosal drug and vaccine delivery. *Eur J Pharm Sci.* 2001;14:201–7.
45. Harleman DRF, Murcott SE. Method of drinking water treatment with natural cationic polymers, US 5543056 A. 1996, Aug 6.
46. Manca ML, Mourtas S, Dracopoulos V, Fadda AM, Antimisariis SG. PLGA, chitosan or chitosan-coated PLGA microparticles for alveolar delivery? A comparative study of particle stability during nebulization. *Colloids Surf B: Biointerfaces.* 2008;62:220–31.
47. NIST/SEMATECH e-Handbook of Statistical Methods, <http://www.itl.nist.gov/div898/handbook/>, date (accessed June 2013), (<http://www.itl.nist.gov/div898/handbook/pri/section5/pri5322.htm>).
48. Ma G, Yang D, Zhou Y, Xiao M, Kennedy JF, Nie J. Preparation and characterization of water-soluble N-alkylated chitosan. *Carbohydr Polym.* 2008;74:121–6.
49. Zong Z, Kimura Y, Takahashi M, Yamane H. Characterization of chemical and solid state structures of acylated chitosans. *Polymer.* 2000;41:899–906.
50. Parlati C, Colombo P, Buttini F, Young PM, Adi H, Ammit AJ, et al. Pulmonary spray dried powders of tobramycin containing sodium stearate to improve aerosolization efficiency. *Pharm Res.* 2009;26(5):1084–92.
51. Kendrick AH, Smith EC, Denyer J. Editorial Nebulizers—fill volume, residual volume and matching of nebulizer to compressor. *Respir Med.* 1995;89:157–159.
52. Elhissi A. Liposomes for pulmonary drug delivery: the role of formulation and inhalation device design. *Curr Pharm Des.* 2017;23(3):362–72.
53. Klariæ D, Hafner A, Zubèiæ S, Dürrigl M, Filipoviæ-Grèiæ J. Spray-dried microspheres based on chitosan and and lecithin cyclosporin a delivery system. *Chem Biochem Eng Q.* 2012;26(4):355–64.
54. Costa P, Lobo J. Modeling and comparison of dissolution profiles. *Eur J Pharm Sci.* 2001;13:123–33.
55. Lv H, Zhang S, Wang B, Cui S, Yan J. Toxicity of cationic lipids and cationic polymers in gene delivery. *J Cont Rel.* 2006;114:100–9.
56. Hoskins C, Cuschieri A, Wang L. The cytotoxicity of polycationic iron oxide nanoparticles: common endpoint assays and alternative approaches for improved understanding of cellular response mechanism. *J Nanobiotechnology.* 2012;10:15.
57. Seydoux E, Rodriguez-Lorenzo L, RAM B, et al. Pulmonary delivery of cationic gold nanoparticles boost antigen-specific CD4 + T cell proliferation. *Nanomedicine.* 2016;12:1815–26.